Project B2 (Sfb 787 Nanophotonics, 2008-2011): Modelling of Dynamics of Quantum Dot Lasers and Amplifiers

(i) Electrically modulated edge-emitting quantum dot lasers

A microscopic 5-variable model for quantum dot (QD) lasers, based upon the coupled dynamics of photons, and electrons and holes in the QDs and in the surrounding quantum well (QW) acting as a carrier reservoir was developed [P5, P7, P8]. One goal was the quantitative modeling of the turn-on dynamics and the modulation response of directly modulated edge-emitting QD lasers (a schematic sketch of the laser and the band structure is shown in Fig.2(a) and (b)). To achieve this goal we have

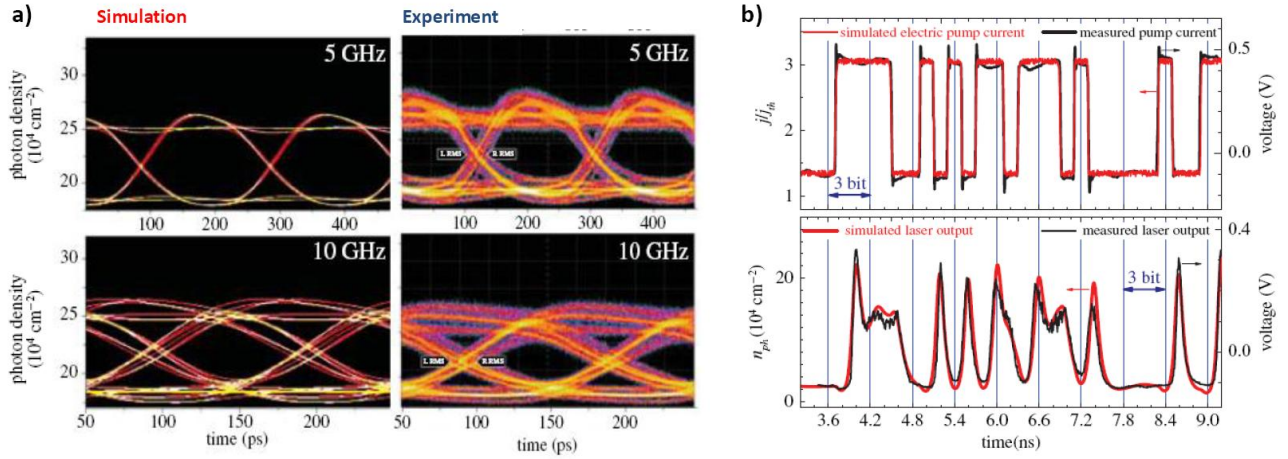

Fig. 1: (a) Simulated and measured eye pattern diagrams for pump currents switching between 4 j_{th} and 6 j_{th} (j_{th}: threshold current density) for bit repetition frequencies of 5 GHz and 10 GHz (b) Simulated (red line) and measured (black line) laser output (bottom) driven by an electric pump signal (top). After [P2].

extended our microscopic rate equation model by including heating effects, pump-dependent spectral properties, and Auger recombination losses in the carrier reservoir [P2]. This has not been done by merely including a static dependence upon the pump current, but rather by a fully self-consistent dynamic dependence on the temperature, the number of longitudinal modes, and the loss rate upon the carrier densities in the reservoir. The latter is calculated dynamically from the coupled rate equations in dependence upon the pump current. Thus we could not only describe correctly the current dependence under continuous-wave (cw) operation, but also predict the transient large-signal response over a large range of pump currents. Figure 1b depicts the simulated and measured laser response to a bit sequence showing the very good quantitative agreement. The quantitative power of the modelling can also be seen by comparing the results to experimental eye diagrams at the emission wavelength of 1.3 µm obtained within the project C6 (Bimberg, Erbert) (see Fig. 1a). We have found that decreasing the injection efficiency into the QW and increasing carrier losses inside the QW at high QW carrier densities is crucial in order to correctly model the large-signal response of the QD laser. Furthermore we have found that an increasing temperature leads to a reduction of the relaxation oscillation frequency and thus to a reduction of the modulation bandwidth at higher pump currents [P2].

Regarding the microscopic basis of our rate equation model we have found that the details of the energy scheme of the QD-QW system sensitively influence the microscopically calculated nonlinear Coulomb scattering rates, and hence the nonlinear turn-on dynamics. We have systematically studied the effects of the electron and hole confinement energies and zero-point energies as well as the doping of the carrier reservoir [P5], and thus we are able to predict changes in the laser dynamics induced by changes in the QD size or QD composition.

A crucial issue for rate equation models is the relation between in- and out-scattering rates. For single-carrier processes in simple two level systems the ratio is constant and only depends upon the temperature T. However, we have derived the detailed balance formula $S_{e/h}^{in,cap} = S_{e/h}^{out,cap} \exp\left[\frac{\Delta E_{e/h}}{kT}\right]\left[\exp\left[\frac{w_{e/h}}{\rho_{e/h} kT}\right]-1\right]$ connecting the non-equilibrium in- and out-scattering Auger rates $S_{e/h}$ (direct capture processes) via a factor that depends on the carrier density $w_{e/h}$ in the

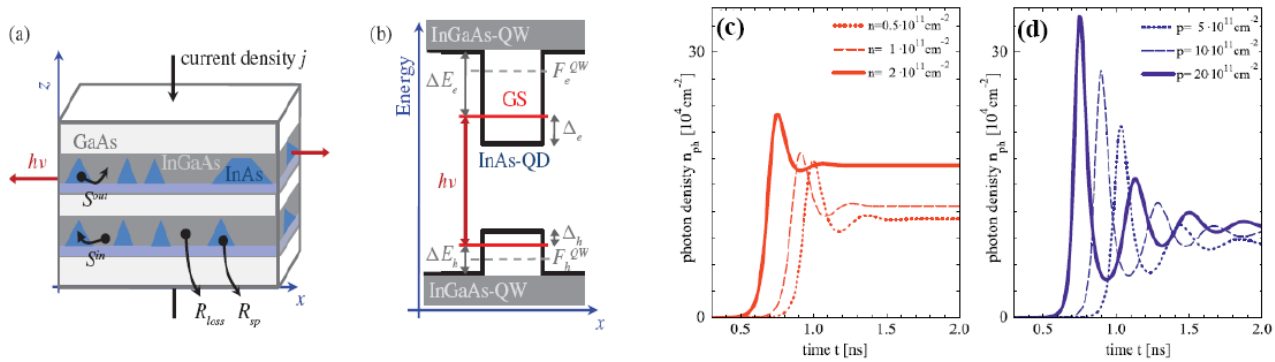

Fig. 2: (a) Sketch of the QD laser structure and (b) of the resulting energy band diagram. (c) and (d) show time series of the photon density during laser turn-on for different n-doping density (c) and different p-doping density (d). Dotted, dashed and solid lines correspond to doping of 0.1, 0.2 and 0.4 times the degeneracy concentration, respectively. Pump current j = 2.5 j_{th}. After [P2, P5].

carrier reservoir [P7] ($\Delta E_{e/h}$ is the energetic distance between the band edge of the reservoir and the confined QD level. The degeneracy concentration of electrons (e) and holes (h) in the reservoir is denoted by $\rho_{e/h}\ kT$ with the 2D density of states $\rho_{e/h}$. We have shown that the inclusion of separate dynamics of holes and electrons is essential in order to explain the dynamic behaviour of a QD laser with a doped carrier reservoir. The dynamics of electrons and holes becomes the more synchronized, the more similar the scattering times (given by the inverse scattering rates) are. However, introducing p-doping drastically reduces the damping of the turn-on relaxation oscillations (see Fig.2d), which is a significant feature influencing the modulation response of these QD lasers [P5]. On the other hand, n-doping increases the damping (Fig.2c).

We have also investigated many-body and nonequilibrium effects upon the dynamical behavior of a QD laser diode. Simulations, based on the Maxwell-Semiconductor-Bloch equations, show strong dependence of the turn-on delay on initial cavity detuning Δ_0 (see Fig.3). This is due to a dynamical shift in the quantum dot distribution caused by bandgap renormalization [P1]. Gain switching behavior is found to be insensitive to inhomogeneous broadening, because the balancing between many-body and free-carrier effects inhibits a cavity resonance walk-off. Both the relaxation oscillation damping and frequency are found to increase with decreasing inhomogeneous broadening widths. However, in contrast to bulk and quantum-well lasers, oscillation damping increases less than the frequency. For applications where control or reproducibility of the turn-on delay is important, it is crucial to have the proper initial cavity detuning with respect to the QD distribution.

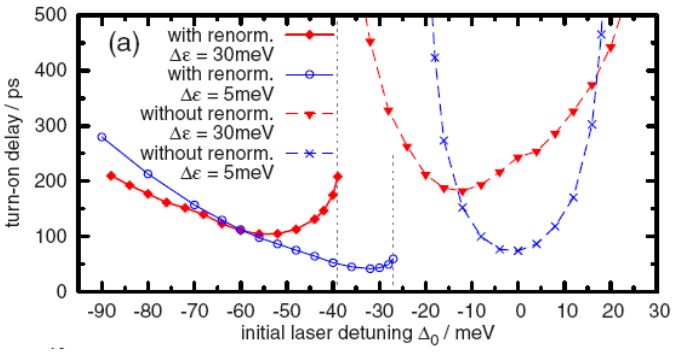

Fig. 3: Turn-on delay vs. initial cavity detuning with (solid) and without (dashed) many-body effects for inhomogeneous broadening of 5 and 30 meV. After [P1].

Another goal of our project was the investigation of a quantum dot laser subjected to optical feedback. For this purpose we combined a Lang-Kobayashi like field equation with the microscopically based carrier rate equations. By tuning the phase-amplitude coupling and the optical confinement factor we were able to discuss various scenarios of the dynamics, and compare them with conventional quantum well lasers. Due to the optical feedback, multistability occurs in our model in form of external cavity modes or delay-induced intensity pulsations. External cavity modes are the basic solutions of the dynamical equations having constant carrier and photon densities and a phase that varies linearly in time. Thus they correspond to cw operation of the laser with feedback. In dependence of the feedback strength we analyzed complex bifurcation scenarios for the intensity of the emitted laser light as well as time series, power spectra and phase portraits of all dynamic variables in order to elucidate the internal dynamics of the laser [P6]. Further we compared our QD to a QW model consisting of a similar field equation but only one carrier-equation for the density of electron-hole pairs. We found that for the same damping of the relaxation oscillations (RO) both lasers become unstable at the same value of the feedback strength in a supercritical Hopf bifurcation. As a result we could explain the reduced feedback sensitivity found in QD devices on the one hand by their strongly damped relaxation

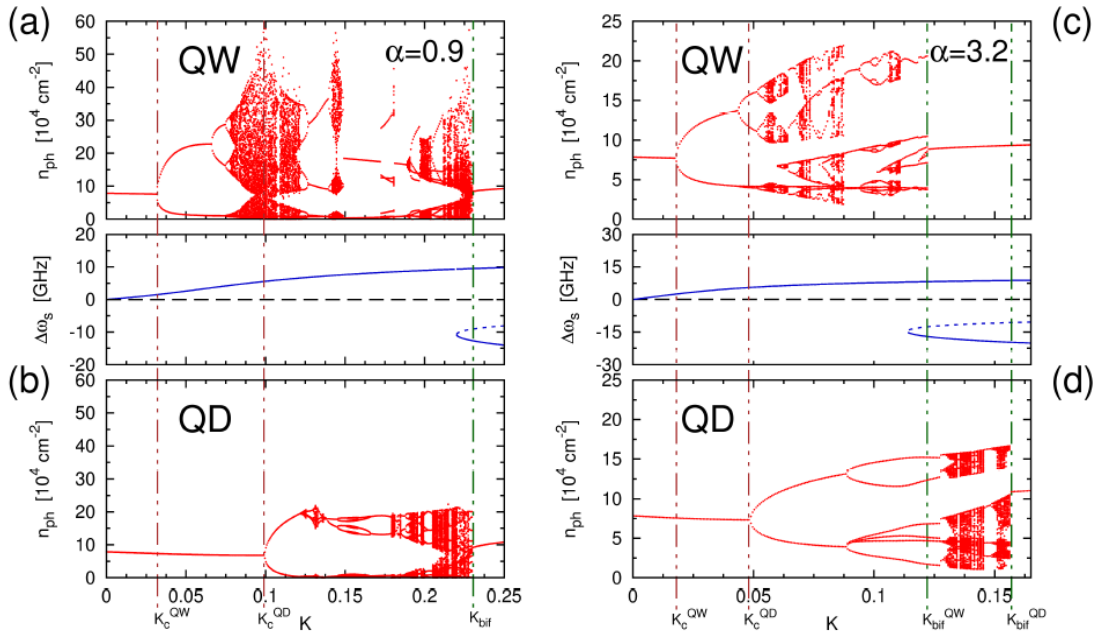

oscillations and on the other hand by the relatively small number of external cavity modes for a given external cavity round trip time. The small number of external cavity modes originates from a weaker

Fig. 4: First bifurcation cascades of the photon density (red) for a QW laser (upper panels) and a QD laser (lower panels) in dependence of the feedback strength K for α=0.9 ((a)-(b)) and α= 3.2 ((c)-(d)). Middle panels: Frequency deviations of the possible external cavity modes (blue). Brown vertical dash-dotted lines mark the Hopf bifurcation. Green vertical dash-dotted lines mark the ends of the bifurcation cascades. After [P6].

phase-amplitude coupling modelled by smaller linewidth enhancement factor (α-factor [1,2]) compared to quantum well devices [P6]. For QD lasers with large α-factor we found bifurcation cascades leading to chaotic regions alternating with short regions of stable cw operation. This resembles the behavior typical for QW devices. For low α-factor the model exhibits reduced feedback sensitivity and performs stable cw operation over a wide range of increasing feedback strength (Fig. 4). Moreover, for low α-factor we found intensity pulsations in a certain range of the feedback strength, which can be strictly regular. They become more irregular with increasing α-factor.

Since the systematic numerical study of the QD laser with optical feedback revealed that damping Γ_{RO} and frequency ω_{RO} of the relaxation oscillations (RO) are crucial for the feedback sensitivity we performed analytical investigations that aimed at understanding the interplay between scattering times and relaxation oscillations. Our analytical approximations are in very good agreement with numerical simulations. They show that the RO frequency does not explicitly depend on the details of the carrier-carrier scattering between QW and QD but strongly depends on the cavity lifetime $1/(2\kappa)$ and radiative recombination lifetime $1/W$. In contrast, the damping rate is crucially affected by the carrier-carrier scattering rates. For equal lifetimes of electrons and holes the damping increases with decreasing lifetimes. If both carrier types have different lifetimes τ_e and τ_h only the slowest species determines the damping rate while the effect of the fast species is negligible. For the case of fast holes and slow electrons that is important for comparison with experiments we found the following analytic relations using asymptotic techniques: $\omega_{RO} = \sqrt{2N_{ph}W\kappa}, \quad \Gamma_{RO} \approx \frac{1}{2}\omega_{RO}{}^2\tau_h + \tau_e^{-1} + W(N_{ph} + N_h)$ where N_{ph} and N_h are the steady state values of the number of photons per QD and the occupation probability of the holes in the QD, respectively. This dependence of Γ_{RO} on τ_e and τ_h is in agreement with our investigations of QD lasers with doped carrier reservoir [P5], where we showed that increasing n-doping concentration leads to a decrease of the electron lifetime τ_e, which was at the same time accompanied by an increased damping. On the other hand, p-doping of the same device did not yield a higher RO damping, which is also explained by the analytics as decreasing the lifetime of the fast species (here the holes) does not significantly change the damping. As a consequence we are able to predict the performance of a QD laser, for instance, n-doping should be helpful to achieve high RO damping rates and thus flat modulation response curves.

(ii) Quantum dot semiconductor optical amplifiers (QD-SOAs)

The second part of the project B2 considered the modelling of quantum dot based optical amplifiers and was aimed at understanding their ultrafast gain recovery dynamics. Due to the very short timescales (fs) found in the gain dynamics it was necessary to use a full nonlinear simulation of the coupled coherent polarization and population dynamics of carriers [P4]. Thus we used the semiconductor Bloch equations including microscopically calculated carrier-carrier scattering rates between the 2D carrier reservoir and the confined QD states. Our results were in good agreement with experiments on the gain recovery and the amplification of pulse trains performed in project C8 (Woggon). The ultrashort gain depletion was found to be sensitive against changes of the pulse area and the dephasing time of the microscopic polarization, while the injection current density mainly influences the non-coherent part of the gain recovery dynamics. A detailed analysis of the underlying carrier dynamics using phase space projections revealed desynchronized behavior of electrons and holes in the recovery dynamics of the QD SOA that is directly related to the different microscopic scattering rates [P4].

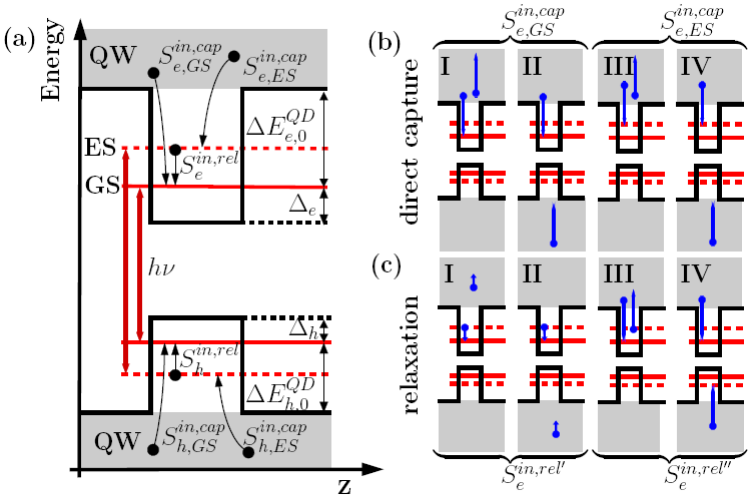

Fig. 5: (a) Energy diagram of the QD-QW system. (b) and (c) show direct electron capture and relaxation processes, respectively, from the QW to the GS (I,II) and the ES (III,IV). Panels I, III and panels II, IV show pure e-e and mixed e-h scattering processes, respectively. After [P3].

In a further step, we extended our model to include the first excited state (ES) of the QDs in addition to the QD ground state (GS) as shown in the band diagram in Fig.5a [P3]. By following the microscopic approach used before for the shallow QD (only one confined level in the QDs [P7]) we systematically included all possible Auger scattering processes between QW, ES and GS. We used microscopically based scattering rates obtained on the basis of a time-dependent perturbation approach [15]. The possible electron transitions that have been considered are shown in Fig. 5b for direct capture processes and in Fig.5c for relaxation processes with the blue arrows. The simulated gain recovery dynamics resulting from the extended model is plotted in Fig.6a for the three different Coulomb scattering channels sketched in Fig.6b. For case 1 we considered only direct capture processes, for case 2 direct capture into ES and relaxation into GS and for case 3 the complete set of all scattering processes. The in-scattering Coulomb rates that were implemented for relaxation processes between ES and GS, and for direct capture into the GS and ES are shown in Fig.6c and Fig.6d, respectively, as a function of the electron density w_e in the carrier reservoir. Note that all these Coulomb scattering processes involve two carriers (Auger processes). By analyzing the different scattering contributions that result from direct capture processes and from relaxation processes (see Fig.6a and b) we could show that the cascading process, where the carriers from the reservoir relax via the excited state makes a major contribution to the ultrafast recovery dynamics [P3]. Since this issue of direct capture and relaxation rates is controversially discussed in the literature, our microscopically based

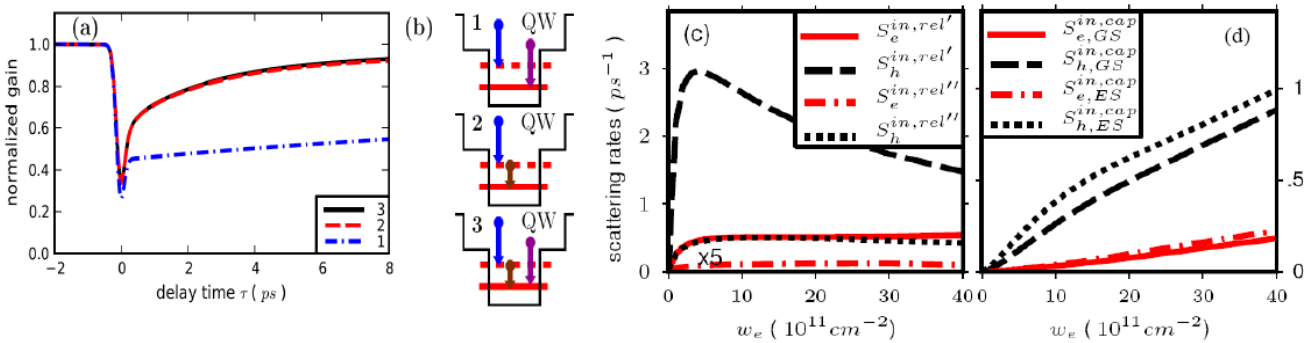

Fig. 6: (a) Ultrafast gain dynamics of QD optical amplifier for scattering scenario 1 (dash-dotted), 2 (dashed) and 3 (solid) as sketched in (b). Panels (c) and (d): Microscopically calculated Coulomb relaxation in-scattering processes between ES and GS $S^{in,rel}_{e/h}$, and in-scattering rates for capture into GS and ES $S^{in,cap}_{e/h,GS/ES}$, respectively, vs. QW carrier densities. After [P3].

calculations could provide answers to those questions that might be of great general interest.

References:

[1] H. Haug: *Optical Nonlinearities and Instabilities in Semiconductors*, Academic Press, (1988).

[2] C. H. Henry: *Theory of the linewidth of semiconductor lasers,* IEEE J. Quantum Electron. **18**, 259 (1982).

[3] J. Yang, P. Bhattacharya, and Z. Wu: *Monolithic integration of InGaAs-GaAs quantum-dot laser and quantum-well electroabsorption modulator on silicon*, IEEE Phot. Technol. Lett. **19**, 747 (2007).

[4] O. Qasaimeh, K. Kamath, P. Bhattacharya, and J. Phillips: *Linear and quadratic electro-optic coeffcients of self-organized* $In_{0.4}\ Ga_{0.6}$ *As/GaAs quantum dots,* Appl. Phys. Lett. **72**, 1275 (1998).

[5] H. N. Klein, H. Chen, D. Hoffmann, S. Staroske, A. G. Steffan, and K. O. Velthaus: 1.*55 µm Mach-Zehnder modulators on InP for optical 40/80 Gbit/s transmission networks*, Conference Proceedings, 2006 International Conference on Indium Phosphide and Related Materials, **171** IEEE, Princeton, NJ, USA, (2006).

[6] V. Flunkert and E. Schöll: *Suppressing noise-induced intensity pulsations in semiconductor lasers by means of time-delayed feedback,* Phys. Rev. E **76**, 066202 (2007).

[7] M. Gioannini, A. Sevega, and I. Montrosset: *Simulations of differential gain and linewidth enhancement factor of quantum dot semiconductor lasers,* Opt. Quantum Electron. **38,** 381 (2006).

[8] W. W. Chow, and S. W. Koch: *Theory of semiconductor quantum-dot laser dynamics*, IEEE J. Quantum Electron. **41**, 495 (2005).

[9] V. Keldysh: *The Effect of a Strong Electric Field on the Optical Properties of Insulating Crystals,* J. Exp. Theo. Phys. **34**, 788 (1958).

[10] D. A. B. Miller, D. S. Chemla, T. C. Damen, A. C. Gossard, W. Wiegmann, T. H. Wood, and C. A. Burrus: *Band-edge electroabsorption in quantum well structures: The quantum-confined Stark effect*, Phys. Rev. Lett. **53**, 2173 (1984).

[11] J. D. Dow and D. Redfield: *Electroabsorption in semiconductors: The excitonic absorption edge*, Phys. Rev. B **1**, 3358 (1970).

[12] D. Merbach, E. Schöll, W. Ebeling, P. Michler, and J. Gutowski: *Electric field dependent absorption of ZnSe-based quantum wells: the transition from two-dimensional to three-dimensional behavior,* Phys. Rev. B **58**, 10709 (1998).

[13] K. E. Callan, L. Illing, Z. Gao, D. J. Gauthier, and E. Schöll: *Broadband chaos generated by an opto-electronic oscillator*, Phys. Rev. Lett. **104**, 11, 113901 (2010) (*highlighted in* Nature **465**, 41 (2010)).

[14] S. Melnik, G. Huyet, and A. V. Uskov: *The linewidth enhancement factor of quantum dot semiconductor lasers*, Opt. Express **14**, 2950 (2006).

[15] T. R. Nielsen, P. Gartner, and F. Jahnke: *Many-body theory of carrier capture and relaxation in semiconductor quantum-dot laser*s, Phys. Rev. B **69**, 235314 (2004).

[16] D. O'Brien, S. P. Hegarty, G. Huyet, and A. V. Uskov: *Sensitivity of quantum-dot semiconductor lasers to optical feedback,* Opt. Lett. **29**, 1072 (2004).

[17] V. Cesari, P. Borri, M. Rossetti, A. Fiore, and W. Langbein: *Refractive index dynamics and linewidth enhancement factor in p-doped InAs-GaAs quantum-dot amplifiers,* IEEE J. Quantum Electron. **45**, 579 (2009).

[P1] B. Lingnau, K. Lüdge, E. Schöll, and W. W. Chow, *Many-body and nonequilibrium effects on relaxation oscillations in a quantum-dot microcavity laser,* Appl. Phys. Lett. **97,** 111102 (2010)

[P2] K. Lüdge, R. Aust, G. Fiol, M. Stubenrauch, D. Arsenijevic, D. Bimberg and E. Schöll, *Large Signal Response of Semiconductor Quantum-Dot Lasers*, IEEE J. Quantum Electron. **46**, 1755, (2010)

[P3] N. Majer, K. Lüdge, and E. Schöll, *Cascading enables ultrafast gain recovery dynamics of quantum dot semiconductor optical amplifiers*, Phys. Rev. B 82, 235301 (2010)

[P4] M. Wegert, N. Majer, K. Lüdge, S. Dommers-Völkel, J. Gomis-Bresco, A. Knorr, U. Woggon, and E. Schöll, *Nonlinear gain dynamics of quantum dot optical amplifiers*, Semicond. Sci.Technol. **26**, 014008 (2011), invited paper.

[P5] K. Lüdge and E. Schöll, *Nonlinear dynamics of doped semiconductor quantum dot lasers,* Eur. Phys. J. D **58**, 167 (2010), invited paper.

[P6] C. Otto, K. Lüdge, and E. Schöll, *Modeling quantum dot lasers with optical feedback: sensitivity of bifurcation scenarios,* Phys. Stat. Sol. (b) **247**, 829 (2010), invited paper.

[P7] K. Lüdge and E. Schöll, *Quantum-dot lasers – desynchronized nonlinear dynamics of electrons and holes,* IEEE J. Quantum Electron. **45**, 1396 (2009), invited paper.

[P8] K. Lüdge, M. J. P. Bormann, E. Malic, P. Hövel, M. Kuntz, D. Bimberg, A. Knorr, and E. Schöll, *Turn-on dynamics and modulation response in semiconductor quantum dot lasers,* Phys. Rev. B **78**, 035316 (2008)